

Catalysis Science & Technology

Accepted Manuscript

This article can be cited before page numbers have been issued, to do this please use: H. Kim, A. A. Eissa, S. B. Kim, H. Lee, W. Kim, D. J. Seo, K. Lee and W. L. Yoon, *Catal. Sci. Technol.*, 2021, DOI: 10.1039/D1CY00485A.



This is an Accepted Manuscript, which has been through the Royal Society of Chemistry peer review process and has been accepted for publication.

Accepted Manuscripts are published online shortly after acceptance, before technical editing, formatting and proof reading. Using this free service, authors can make their results available to the community, in citable form, before we publish the edited article. We will replace this Accepted Manuscript with the edited and formatted Advance Article as soon as it is available.

You can find more information about Accepted Manuscripts in the [Information for Authors](#).

Please note that technical editing may introduce minor changes to the text and/or graphics, which may alter content. The journal's standard [Terms & Conditions](#) and the [Ethical guidelines](#) still apply. In no event shall the Royal Society of Chemistry be held responsible for any errors or omissions in this Accepted Manuscript or any consequences arising from the use of any information it contains.

Article type: Full Paper

View Article Online
DOI: 10.1039/D1CY00485A

One-Pot Synthesis of Highly Mesoporous Ni/MgAl₂O₄ Spinel Catalyst for Efficient Steam Methane Reforming: Influence of Inert Annealing

Hyunjoung Kim^{a,1}, Ahmed Al-Shahat Eissa^{a,b,1}, Seung Bo Kim^a, HongJin Lee^a, Woohyun Kim^c, Dong Joo Seo^c, Kyubock Lee^{a,*} and Wang Lai Yoon^c

^a Graduate School of Energy Science and Technology, Chungnam National University, 99 Daehak-ro, Yuseong-gu, Daejeon 34134, Republic of Korea

^b Department of Chemistry, School of Science, South Valley University, Qena 83523, Egypt

^c Hydrogen Research Department, Korea Institute of Energy Research, 152 Gajeong-ro, Yuseong-gu, Daejeon 34129, Republic of Korea

* Corresponding author: kyubock.lee@cnu.ac.kr

¹ These authors contributed equally to this work.

Abstract

A highly mesoporous Ni/MgAl₂O₄ spinel catalyst was facilely synthesized by a scalable one-pot strategy and employed in steam methane reforming (SMR) reaction. The influence of annealing the catalyst in N₂ atmosphere on its structural properties and catalytic performance is fully demonstrated for the first time. Physical characterizations showed that subjecting the catalyst to an inert-annealing process (e.g., in N₂ atmosphere) before calcining it in air enhances the specific surface area (SSA) and mesoporosity, improves the dispersion of Ni nanoparticles (NPs) within the support matrix, boosts the interaction between the active phase and support, and increases the content of the reduced Ni species on the catalyst surface. With its remarkable structural properties, the catalyst exhibits high CH₄ conversion efficiency and durability as well as superb resistance to carbon deposition. These results reveal that the substructure and catalytic activity of the catalyst can be tuned by controlling the annealing conditions during the synthesis process. The straightforwardness of the synthesis strategy employed in this work makes it a promising route for designing catalysts with high coke-resistance in reforming and other high-temperature Ni-catalyzed reactions.

Keywords

View Article Online
DOI: 10.1039/D1CY00485A

Steam methane reforming, one-pot synthesis, inert annealing, mesoporosity, Ni/MgAl₂O₄ catalyst.

1. Introduction

The main source of energy is still fossil fuels, which are non-renewable and have detrimental effects on our environment,¹ due to the generation of huge amounts of greenhouse gases upon the combustion of fossil fuels. On contrary, hydrogen (H₂) is an attractive energy carrier with high energy density (~ 122 kJ g⁻¹), which can be utilized in fuel cells to generate clean energy with high efficiency to operate portable devices and transportation systems.² As a result, the global demand for H₂ is growing very fast. H₂ production from natural gas is positioned as a transition point between fossil fuel and renewable energy systems. SMR is one of the most common and effective commercialized processes to produce H₂, meeting almost 50% of the worldwide need for H₂.^{3,4} SMR is a process that results in the formation of syngas (a gaseous mixture of CO and H₂) through a highly endothermic reaction between methane (CH₄) and water vapor (H₂O).^{5,6} Syngas has long been used in energy production applications as well as the synthesis of valuable chemicals through the Fischer-Tropsch reaction.^{7, 8}

Noble metals such as ruthenium (Ru), rhodium (Rh), and platinum (Pt) provide high catalytic activity suitable for the SMR reaction,⁹ however, their scarceness and high cost hinder their commercial applications. Hence, the development of efficient noble-metal-free catalysts is of utmost importance. Currently, nickel (Ni) is the most preferred catalyst for the SMR reaction as well as dry methane reforming, due to its superb reactivity and low cost.^{10–13} However, the development of supported Ni-based catalysts with higher resistance against the carbon deposition and thermal aggregation of Ni NPs during the long-term high-temperature reaction conditions remains a major challenge.¹⁴ It is noteworthy that the durability of Ni-based catalysts depends on the nature of support, the interaction between the metallic Ni phase and

the support, and the size of Ni NPs.¹⁵ Indeed, carbon-deposition reactions (CH_4 direct decomposition, the Boudouard reaction, etc.) happen more readily on large Ni crystallites, which are created due to the high operating temperature required for proceeding the SMR reaction, where the Ni NPs easily agglomerate.¹⁶ Therefore, reducing the Ni crystal size is regarded as one of the most successful strategies for enhancing the catalyst stability. The confinement of well-dispersed Ni-active phase within the mesopores of stable supports such as alumina (Al_2O_3)^{4, 17–21} is an effective approach to minimize Ni agglomeration during the SMR reaction, and hence maintaining high reactivity for prolonged periods under the harsh operating conditions. The optimum support should be resistant to high temperature and must maintain good metal dispersion during the reaction. In this regard, the magnesium aluminate spinel (MgAl_2O_4) is a promising candidate as an efficient support in many catalytic applications,^{4, 22–28} due to its high mechanical strength, high melting temperature (2408 K), admirable chemical durability, and high thermal stability.^{29,30} More importantly, the incorporation of a basic metal (Mg) into the substructure of the comparatively acidic Al_2O_3 inhibits the carbon deposition and promotes the dispersion of the active Ni species within the support.³¹

In the present study, we report a one-pot synthesis strategy for producing Ni NPs supported on highly mesoporous MgAl_2O_4 spinel catalyst, where mesoporous MgAl_2O_4 was used as a support for the confinement of the well-dispersed Ni-active phase, due to its low acidity, high sintering resistance, and robust interaction of the metal with MgAl_2O_4 support, all giving rise to efficient catalysts for the SMR reaction. The catalyst was fabricated by “one-pot” evaporation-induced self-assembly (EISA) method, then inert annealing in N_2 atmosphere at 800 °C for 2.0 h, was performed on the as-synthesized sample before normal calcination step in air to remove the sacrificial template. The influence of inert annealing in N_2 atmosphere on the structural properties and catalytic activity of the catalyst is elucidated for the first time. Through the careful investigation of the structure-performance relationship of the catalysts, it

View Article Online
DOI: 10.1039/D1CY00485A

was found that the catalyst annealed in N₂ atmosphere at 800 °C exhibited the superior CH₄ conversion efficiency and minimum carbon deposition, due to the high surface area, high mesoporosity which facilitates the flow of reactants to the active sites, robust interaction of Ni NPs with the MgAl₂O₄ support, and the homogeneous dispersion of the Ni NPs on the support.

View Article Online
DOI: 10.1039/D1CY00485A

2. Experimental

2.1 Materials

Aluminum iso-propoxide (Al(OiPr)₃, ≥98%), magnesium nitrate hexahydrate (Mg(NO₃)₂·6H₂O, ≥98%), and nickel nitrate hexahydrate (Ni(NO₃)₂·6H₂O, ≥98%) were purchased from Sigma-Aldrich, USA, and used as sources of Al, Mg, and Ni, respectively. Absolute ethanol (C₂H₅OH, ≥98%, Samchun, Korea) and nitric acid (HNO₃, 60.0%, Samchun, Korea) were used as solvents. Tri-block co-polymer Pluronic P123 (EO₂₀PO₇₀EO₂₀, molecular weight = 5800 g mol⁻¹, Sigma-Aldrich, USA) was used as a structure-directing agent. All of the chemicals were utilized as received without any further purification.

2.2 Synthesis of catalysts

The catalysts were synthesized using EISA method as shown in the schematic illustration of Fig. 1. Firstly, 6.32 g of P123 were added to a mixture consisting of 138.16 mL of ethanol and 10.4 mL of HNO₃ under a stirring rate of 700 rpm for 12.0 h. Secondly, Al(OiPr)₃, Mg(NO₃)₂·6H₂O, and Ni(NO₃)₂·6H₂O were added to the above solution and stirred for additional 6.0 h. The mixing molar ratios of all of the components were fixed at 1 : 0.017 : 35 : 1.94 for (Al(OiPr)₃ + Mg(NO₃)₂·6H₂O + Ni(NO₃)₂·6H₂O) : P123 : C₂H₅OH : HNO₃. The precursor solution was dried at 60 °C for 48.0 h in an oven, carbonized in N₂ atmosphere at 800 °C for 2.0 h, calcined in air at the same temperature for another 2.0 h, then finally, reduced in H₂/N₂ atmosphere at 800 °C for 2.0 h before the catalytic reaction. The obtained catalyst was named O–Ni/MgAl₂O₄/Inert/Air, where ‘O’ refers to one-pot. For convenience, we named this material O–NMA/Inert/Air, where N indicates Ni, M indicates Mg, and A indicates aluminate

(Al₂O₄) (Fig. 1c). Another sample was fabricated using the same procedure except without annealing in N₂ atmosphere, and named O–NMA/Air (Fig. 1b). A third sample was prepared by loading Ni, via a conventional incipient wetness impregnation method, where the dried gel obtained by EISA method was calcined in air at 800 °C for 2.0 h, then impregnated with Ni. Finally, the solid was calcined again in air at 800 °C for 2.0 h, then reduced in H₂/N₂ atmosphere at 800 °C for 2.0 h, before the SMR reaction. This sample was named as I–NMA, where ‘I’ indicates impregnation (Fig. 1a). The weight percent (wt%) of Ni in all catalysts was fixed at 18 wt%. The obtained powder was pelletized under 200 bar, then ground and sieved to obtain particles of 149–177 μm size for use in the catalytic reaction.

2.3 Physical characterization of catalysts

A Brunauer–Emmett–Teller (BET) analysis was performed using BELSORP-mini (MicrotracBEL, Japan). The samples were pretreated in a vacuum at 300 °C for 3.0 h, then subjected to nitrogen adsorption-desorption at –196 °C. The pore-size distribution was analyzed according to the Barrett-Joyner-Halenda (BJH) theory. Inductively coupled plasma atomic emission spectroscopy (ICP-AES) analysis was performed to determine the chemical composition of the as-synthesized catalysts using the Avio500 (Perkin-Elmer, USA). X-ray diffraction (XRD) analysis was performed using an AXS D8 diffractometer (Bruker, USA) at Cu Kα wavelength, 40 kV, and 40 mA. The crystallite size of Ni⁰ NPs was calculated using Scherrer equation:²

$$\text{Ni}^0 \text{ crystallite size} = (K \times \lambda) / (\beta \times \cos \theta)$$

where K is a shape factor, λ is the wavelength of the X-ray source, β is the full width at half-maximum in radian, and θ is the peak position in radians. Transmission electron microscopy (TEM) analysis was performed using JEM-2100F (JEOL, Japan) at 200 kV at the National Nanofab Center in Korea. The reduction properties of the catalysts were analyzed by hydrogen-temperature programmed reduction (H₂-TPR) using the BET-CAT (MicrotracBEL, Japan). The

analysis was performed at temperatures ranging from 50 to 1000 °C under 5% H₂/Ar atmosphere after the pretreatment at 200 °C under He atmosphere. For determining the reduction degree, the amount of consumed H₂ for reducing each catalyst was calculated in the range 50 – 800 °C. 800 °C was selected as the pre-reduction step before the SMR reaction, then the reduction degree was calculated from integrating the peak areas under the TPR profiles at 800 °C and 1000 °C according to the following equation:

$$\text{Reduction degree (\%)} = \text{H}_2 \text{ amount consumed at 800 °C} / \text{H}_2 \text{ amount consumed at 1000 °C}.$$

The dispersion of active Ni⁰ was estimated by using H₂-chemisorption method (Auto chem II 2920 Micromeritics). Before the estimation, the samples were reduced under 5 vol% H₂/Ar at 800 °C for 3 h. The amount of chemisorbed hydrogen molecules on Ni⁰ was measured at 50 °C under the pressure from 0 mmHg to 600 mmHg. For calculating the dispersion of Ni⁰ (*D* (%)) under the assumption of the stoichiometry between hydrogen molecules and Ni⁰ on the surface of the catalyst to be 1:1, the following equation was used:

$$D (\%) = \frac{V_{H_2,Chem} \times SF \times MW_{Ni}}{W_{sample} \times WF_{Ni} \times MV_{H_2,STP}} \times 100$$

where $V_{H_2,Chem}$ is the volume of chemisorbed hydrogen (mL) on Ni⁰ under the standard temperature and pressure (STP) conditions. The dimensionless value, stoichiometry factor, *SF* is 1. Molecular weight of Ni, MW_{Ni} , is 58.69 g/mol. The weight of the sample (g) is denoted as W_{sample} . The weight fraction of Ni, WF_{Ni} , is the same (18%) for all samples. The molar volume of H₂ under STP conditions, $MV_{H_2,STP}$, is 22,414 mL/mol.

X-ray photoelectron microscopy (XPS) signals were recorded using a Thermo Scientific K-Alpha XPS system (Thermo Fisher Scientific, UK) equipped with a micro-focused monochromatic Al K α X-ray source (1486.6 eV). A 400 μ m X-ray beam was used at 6 mA \times 12 kV. The spectra were acquired in the constant analyzer energy mode with a pass energy of 400 eV. Thermo Scientific Avantage software (Thermo Fisher Scientific, UK) was used for digital acquisition and data processing. Thermogravimetric analysis (TGA) was performed to

determine the amount of deposited cokes using the Labsys TGA EVO (Setaram Instrumentation, France) at temperatures up to 1000 °C in air. The coke deposits on the surfaces of the catalysts were observed by the field-emission scanning electron microscopy (FESEM, S-4800, Hitachi Co., Japan). Raman spectra of the used catalysts were collected on a LabRAM HR-800 UV-Visible-NIR system equipped with a charge-coupled detector (CCD) and an InGaAs array detector, with a laser wavelength of 514 nm and 1800 Grating, an ND 10% filter, a time of 8 s, and a wavenumber range of 1000 ~ 2000 cm⁻¹.

2.4 Catalytic activity measurements

Catalytic reactions were conducted in a fixed-bed reactor (using a quartz tube of 4 mm internal diameter). Prior to the reaction, the calcined powder was in-situ reduced at 800 °C for 2.0 h under a flow rate of 50 sccm (H₂/N₂=1/4) to obtain the active phase (Ni⁰). The flow was then switched to the reactant mixture (H₂O/CH₄=3/1) at *T*= 800 °C and *P*= 1.0 atm. Water was injected by a Micro pump (NP-KX-200, DONGSUNG science, Korea), wherein it was evaporated at 180 °C, then mixed with the other gases. The total gas hourly space velocity (GHSV) was increased from 10,000 to 40,000 mL g_{cat}⁻¹ h⁻¹ (catalyst weight = 0.085 g). Catalytic reactions in the accelerated deactivation mode, which promote the formation of coke, were performed under the conditions of H₂O/CH₄= 1, *T*= 700 °C, *P*= 1.0 atm., and GHSV= 10,000 mL g_{cat}⁻¹ h⁻¹. The reaction temperature was controlled with a thermocouple located at the center of the catalyst bed. Next, the reactants and products were quantified by on-line gas chromatography (GC) using a HP 6890 GC system (Agilent Technologies Inc., USA) equipped with a thermal conductivity detector. The CH₄ conversion and H₂/CO ratio were calculated using the following equations:

$$\text{CH}_4 \text{ conversion (\%)} = \frac{[\text{CH}_4]_{in} - [\text{CH}_4]_{out}}{[\text{CH}_4]_{in}} \times 100$$

Where $[\text{CH}_4]_{\text{in}}$ and $[\text{CH}_4]_{\text{out}}$ are the inlet and outlet volume flow of CH_4 gas, respectively.

$$\text{H}_2/\text{CO} = \frac{[\text{H}_2]_{\text{out}}}{[\text{CO}]_{\text{out}}}$$

Where $[\text{H}_2]$ and $[\text{CO}]$ are the outlet volume of H_2 and CO gases, respectively.

3. Results and discussion

3.1 Characterization of as-prepared catalysts

BET analyses were performed to determine the SSA and pore size distribution (PSD) for the synthesized materials before and after the reduction process, using N_2 adsorption/desorption isotherms (Fig. 2). As shown in Fig. 2a, b, all the as-synthesized samples presented type-IV isotherms with conspicuous H1-shaped hysteresis loops between the adsorption and desorption segments at higher P/P_0 values (>0.6), which ordinarily are related to capillary condensation and evaporation in mesoporous nanomaterials.³³ Moreover, the hysteresis loops displayed by the synthesized catalysts exhibited a high degree of steepness, indicating the existence of abundant mesopores with premium uniformity within the substructure of the catalysts.³² These valuable characteristics of the isotherms indicate that the as-prepared catalysts had optimum mesoporous structure, which is very fundamental for boosting the catalytic activity of a material. The shift in the loop position to higher relative pressures in the case of I-NMA in Fig. 2b is due to the increase in the size of its mesopores. As shown in Table S1, the catalyst fabricated via the impregnation route (I-NMA) had the minimum BET SSA among the examined samples both before and after the reduction process (156.17 and $98.93 \text{ m}^2 \text{ g}^{-1}$). When the one-pot strategy was applied for synthesizing the material (O-NMA/Air), the BET SSA before the reduction enhanced greatly from 156.17 to $211.18 \text{ m}^2 \text{ g}^{-1}$ (Table S1). This suggests that the synthesis method highly influenced the textural characteristics of the material. When the material was heated in N_2 atmosphere for 2.0 h at $800 \text{ }^\circ\text{C}$ before calcining in air (O-

NMA/Inert/Air), the BET SSA enlarged from 211.18 to 253.08 m² g⁻¹, indicating the great influence of the inert carbonization in increasing the SSA of the material. After the reducing process, the BET SSAs of all materials were decreased; however, the catalyst that had been carbonized in N₂ atmosphere (O–NMA/Inert/Air) maintained the maximum BET SSA (122.49 m² g⁻¹). This clearly demonstrates the importance of this step in promoting the SSA of the catalyst, and hence strengthening its SMR performance, where the high BET SSA provides more accessible active sites during an SMR reaction.

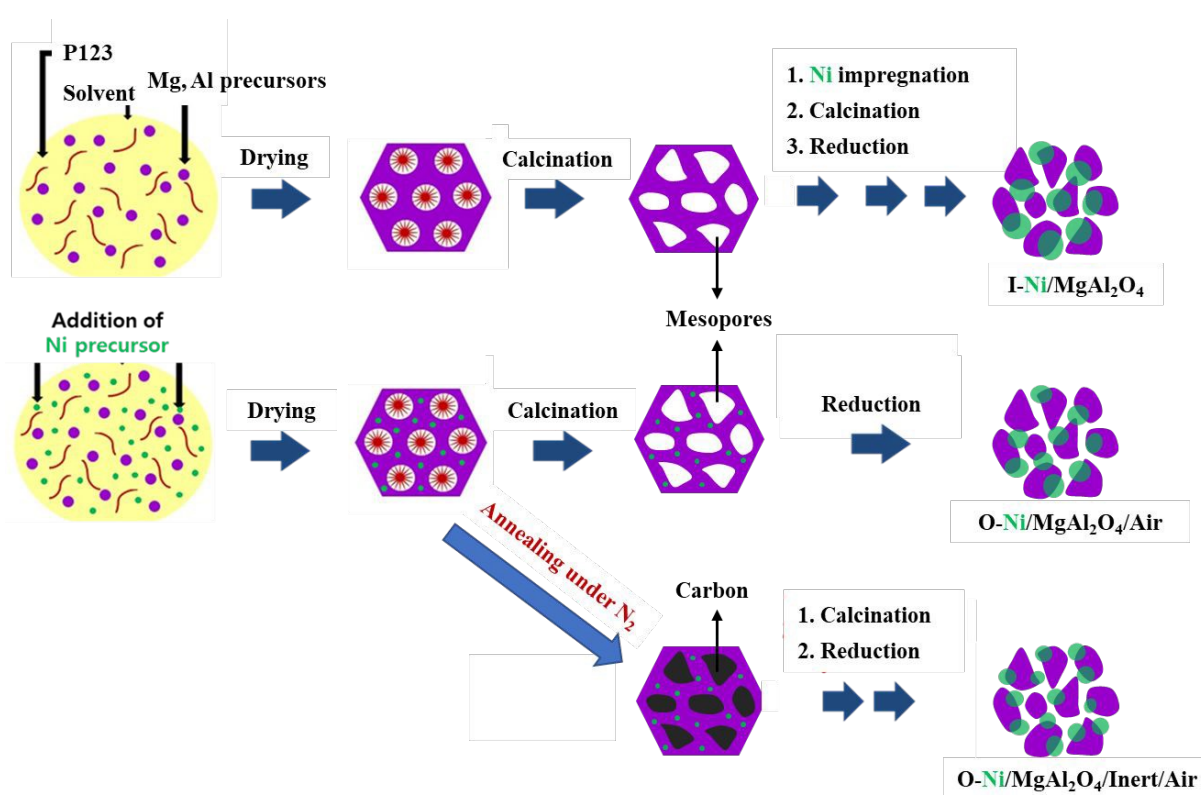


Fig. 1 – Schematic diagram for the synthetic procedures of mesoporous Ni/MgAl₂O₄ catalysts.

Since the O–NMA/Air sample was subjected to a calcination temperature of 800 °C for 4.0 h (2.0 h in air and 2.0 h in H₂/N₂ atmosphere), meanwhile, the sample O–NMA/Inert/Air was subjected to the same temperature but for 6.0 h (2.0 h in N₂, 2.0 h in air, and 2.0 h in H₂/N₂ atmosphere), an additional sample was fabricated by maintaining the calcination temperature for 4.0 h in air (O–NMA/Air_{4h}). When the as-prepared sample was annealed in air for 4.0 h instead

of 2.0 h, the BET SSA decreased from 211.18 to 187.49 $\text{m}^2 \text{g}^{-1}$ and from 104.37 to 83.45 $\text{m}^2 \text{g}^{-1}$ before and after the reduction process, respectively (Fig. S1 and Table S1). Subjecting the material to a longer calcination process offers a greater probability of agglomeration of the NPs, and thus diminishing its SSA as well. Consequently, the O-NMA/Air_{4h} catalysts displayed a smaller SSA than the O-NMA/Air_{2h} sample. Under the established conditions, both O-NMA/Inert/Air and O-NMA/Air_{4h} were subjected to 800 °C for 6 h; however, O-NMA/Inert/Air had a higher BET SSA (122.49 $\text{m}^2 \text{g}^{-1}$) than O-NMA/Air_{4h} (83.45 $\text{m}^2 \text{g}^{-1}$), demonstrating the importance of the inert annealing in promoting the SSA of the material.

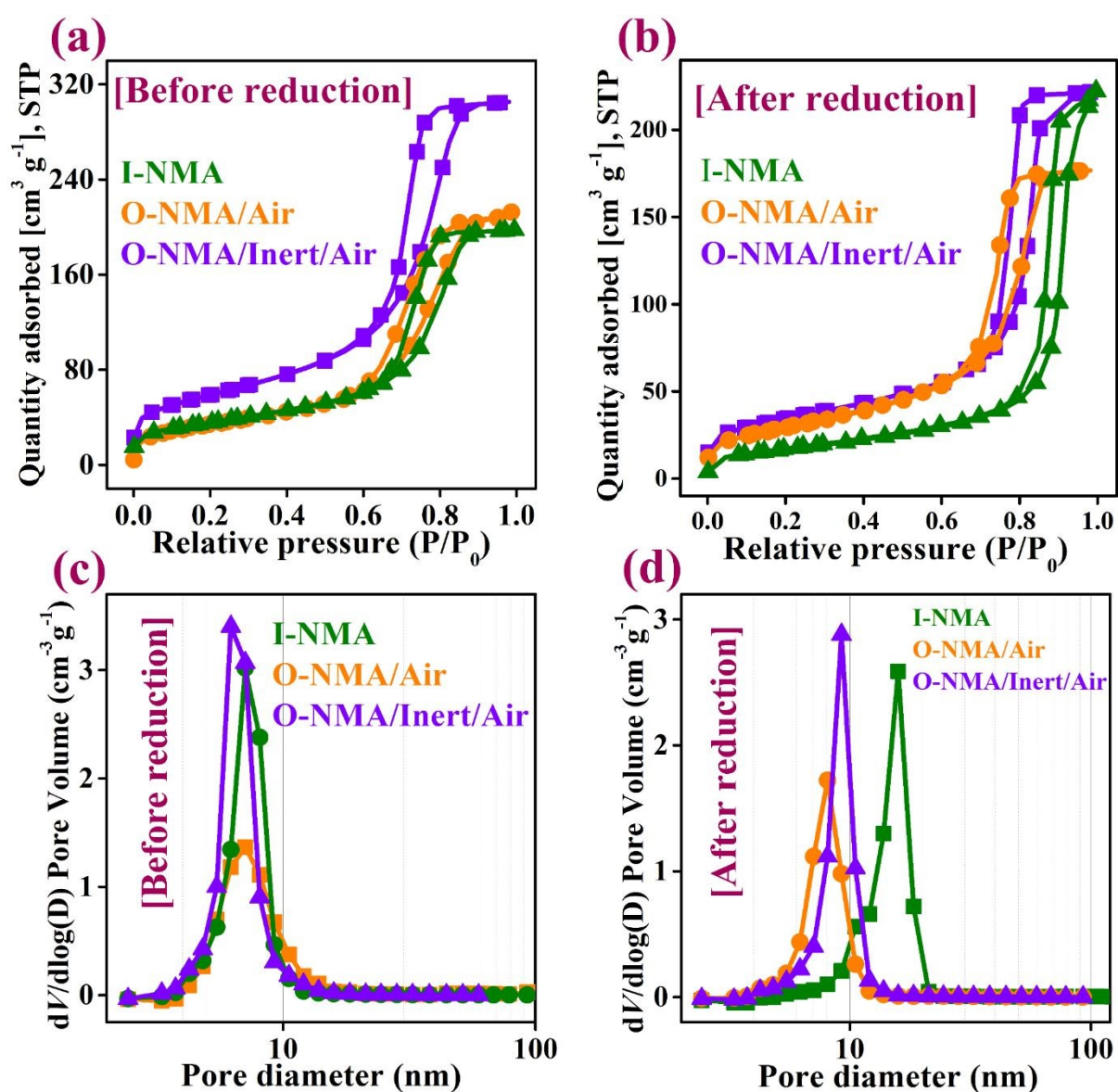


Fig. 2 – N₂ adsorption/desorption isotherms (a, b) and BJH pore-size distributions (c, d) of mesoporous Ni/MgAl₂O₄ catalysts before (a, c) and after reduction (b, d).

View Article Online
DOI: 10.1039/D1CY00485A

The presence of mesopores was emphasized by the PSD curves, obtained from the desorption branches of the isotherms (Fig. 2c, d). All samples exhibit a sharp PSD with one narrow peak existing within the conventional range for uniform mesoporous materials, demonstrating that all samples have a homogenous mesoporous structure.^{34,35} This optimum porosity is very beneficial for improving the catalytic activity.³² The PSD analysis showed that the pore diameters of all calcined catalysts were predominately around 7.65, 8.01, and 6.58 nm for I-NMA, O-NMA/Air, and O-NMA/Inert/Air, respectively, assuring that the high SSAs of the herein as-fabricated materials were due to the mesoporosity (mesopores size: 2.0–50.0 nm based on the IUPAC definition). After reducing the materials, the predominant pore diameter (d) of the I-NMA catalyst increased sharply from 7.65 to 17.63 nm; meanwhile, it slightly increased in the case of the O-NMA/Air and O-NMA/Inert/Air catalysts (Fig. 2c, d and Table S1), indicating that the latter materials had a stable porous structure compared with the former one. The increase in the pore size of I-NMA catalyst after reduction can be explained as follows: In the one-pot synthetic method, Ni was added before fabricating the support and hence it became like a main part of the support. This resulted in strong interaction of Ni NPs with the support, where the Ni NPs were fixed within the pores of the support. As a result, the obtained catalysts prepared by one-pot strategy (O-NMA/Air and O-NMA/Inert/Air) had a stable pore structure with robust interaction with the Ni NPs, which prevents their agglomeration. On the other hand, the impregnation method involves two steps for synthesizing the catalyst: the first step involves synthesizing the support, and second step involves impregnating the support with Ni. In that case, the formed Ni NPs were not strongly interacted with the support, and hence easily agglomerated during the reduction step, which resulted in deteriorating the pores of the support, where the pores cannot sustain the extension in the size

of Ni NPs, and therefore they deteriorated and increased in size. This has been confirmed from the XRD data where the size of Ni NPs was maximum in the case of I-NMA catalyst and minimum O-NMA/Inert/Air catalyst (Table 1). This observation clarifies the importance of one-pot method in preparing the catalyst in the terms of obtaining a stable porous structure, strong interaction of the active phase with the support, and small size of the NPs.

Furthermore, the pore volume of O-NMA/Inert/Air was the highest among the synthesized catalysts before ($0.5814 \text{ cm}^3 \text{ g}^{-1}$) and after ($0.3433 \text{ cm}^3 \text{ g}^{-1}$) the reduction process, which is very helpful for enhancing the mass transfer during the SMR reaction. On the other hand, increasing the annealing time in air from 2.0 h to 4.0 h resulted in 'd' growing from 8.01 to 8.48 nm and from 17.08 to 19.88 nm before and after the reduction process, respectively (Fig. S1 and Table S1). This again emphasizes that the materials prepared by the one-pot method had a more durable porous structure than the materials prepared by two-step methods, where the value of 'd' did not change dramatically after performing the reduction process in the H_2/N_2 atmosphere. The durable porous structure in the case of the O-NMA/Inert/Air catalyst is essential for maintaining the high reactivity of the catalyst during the SMR reaction. From the BET data, it can be concluded that the O-NMA/Inert/Air catalyst had a superb texture structure, which could greatly contribute to boosting its catalytic activity towards the SMR.

Powder X-ray diffraction (XRD) analysis was performed to determine the crystal structure and the nature of the phases existing in the as-prepared samples (Fig. 3). All samples showed clear diffraction peaks indicating the high crystallinity. Before the reduction process, all calcined samples showed comparable patterns regardless of the preparation method, except I-NMA catalyst, which showed two distinct peaks at 2θ of 43.29° and 62.85° , which are assigned to the NiO phase (PDF#01-1239). On the other hand, O-NMA/Inert/Air displayed a very weak NiO-related peak at 2θ of 43.29° , while O-NMA/Air did not show any peaks for NiO phase. The absence of apparent diffraction peaks for NiO phase in O-NMA/Air and O-

View Article Online
DOI: 10.1039/D1CY00485A

NMA/Inert/Air reflects the excellent dispersion of NiO within the substructure of the support. View Article Online
DOI: 10.1039/D1CY00485A

The high intensity of peaks related to the spinel phases is due to the overlapping between the diffraction peaks of the MgAl_2O_4 (PDF#21-1152) and NiAl_2O_4 (PDF#10-0339) crystal phases, since both phases have approximately the same diffraction angles, as can be clearly seen from the reference peaks in Fig. 3. After reducing the materials, the peaks related to the NiO phase in the I-NMA catalyst disappeared. In addition, two prominent diffraction peaks positioned at 2θ of 51.85° and 76.38° , were discerned in all of the catalysts, which are attributed to the formation of the cubic Ni phase (PDF#65-2865). More importantly, the peak located at 2θ of 44.49° showed the maximum intensity among all peaks in all catalysts, owing to the formation of the cubic Ni phase. These observations confirm the success of the reduction process for all samples. It can be clearly seen from the XRD patterns of the catalysts that the intensities of the diffraction peaks related to the spinel phases pronouncedly decreased after completion of the reduction process (Fig. 3b). This was due to the reduction of Ni from the NiAl_2O_4 spinel phase, which corroborates the existence of NiAl_2O_4 spinel species in the synthesized catalysts. Further confirmation will be provided by the H_2 -TPR analysis (see below).

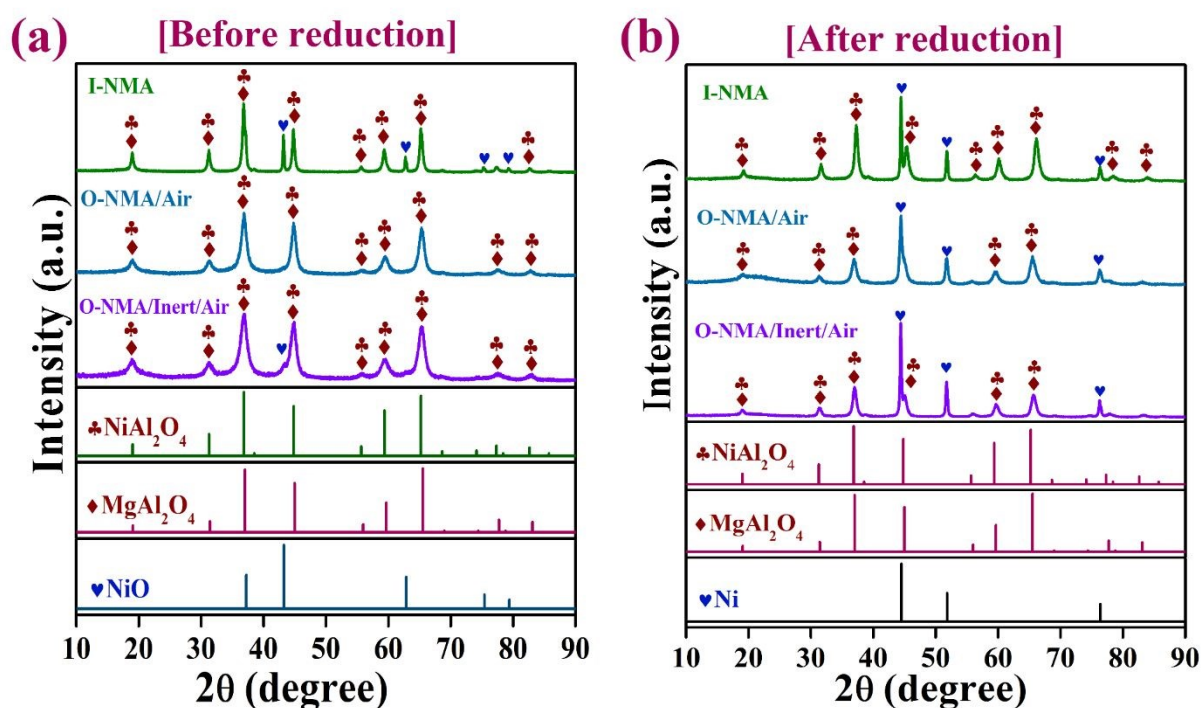


Fig. 3 – PXRD patterns of mesoporous Ni/MgAl₂O₄ catalysts synthesized by different strategies, before (a) and after (b) reduction.

TEM images of the reduced samples are shown in Fig. 4. It is obvious that all the catalysts show mesoporous textures. The Ni NP size distributions reveal that the O–NMA/Inert/Air catalyst had smaller Ni NPs (~ 26.73 nm) distributed on the MgAl₂O₄ support relative to the I–NMA and O–NMA/Air catalysts (NPs size ~ 49.83 and 38.29 nm, respectively). This microscopic observation is in accordance with the calculated Ni crystallite sizes by using Scherrer equation based on the XRD results, namely the smallest Ni crystallite size for the O–NMA/Inert/Air catalyst as summarized in Table 1. Ni reduction degree and Ni dispersion were calculated from the results of H₂-TPR and H₂-chemisorption, respectively (Table 1). The I–NMA, O–NMA/Air, and O–NMA/Inert/Air catalysts showed reduction degrees of 94, 88, and 86%; respectively, indicating that Ni species in O–NMA/Inert/Air catalyst are more difficult to reduce than the other two catalysts. This confirms that Ni species in the latter catalyst has a strong interaction with the support, which will be discussed further in detail. The H₂-chemisorption was performed to evaluate the dispersion degree of Ni active sites for the various catalysts. The O–NMA/Inert/Air catalyst exhibited the maximum degree of Ni dispersion (3.35%) among the examined catalysts, meanwhile I–NMA catalyst showed the minimum one (1.22%). The O–NMA/Air catalyst showed Ni dispersion degree between both I–NMA and O–NMA/Inert/Air catalysts (2.38%). These results prove that Ni species in I–NMA that weakly interacted with the support were reduced to large Ni⁰ NPs, meanwhile, they were reduced into small Ni⁰ NPs in O–NMA/Inert/Air, due to the strong interaction with the support. These results also confirm that quantity of Ni species that were reduced to Ni⁰ NPs in I–NMA was higher than those in O–NMA/Inert/Air, due to the more robust interaction of Ni species with support in the latter one. This indicates that both the synthetic approach and the calcination step in N₂ atmosphere had great influences on the Ni dispersion degree within the support matrix, which would have a fundamental role on the catalytic activity during the SMR

reaction. The number of Ni⁰ active sites was calculated by considering the dispersion of Ni⁰ and the reduction degree.⁴¹ It is clear from Table 1 that O–NMA/Inert/Air displayed the highest number of Ni⁰ active sites among the as-prepared catalysts (8.68×10^{-7} mol). Since O–NMA/Inert/Air showed the highest surface area, lowest NPs size, highest Ni dispersion, and the largest number of Ni⁰ active sites, it was expected that this catalyst will show the best catalytic activity among the herein studied catalysts.

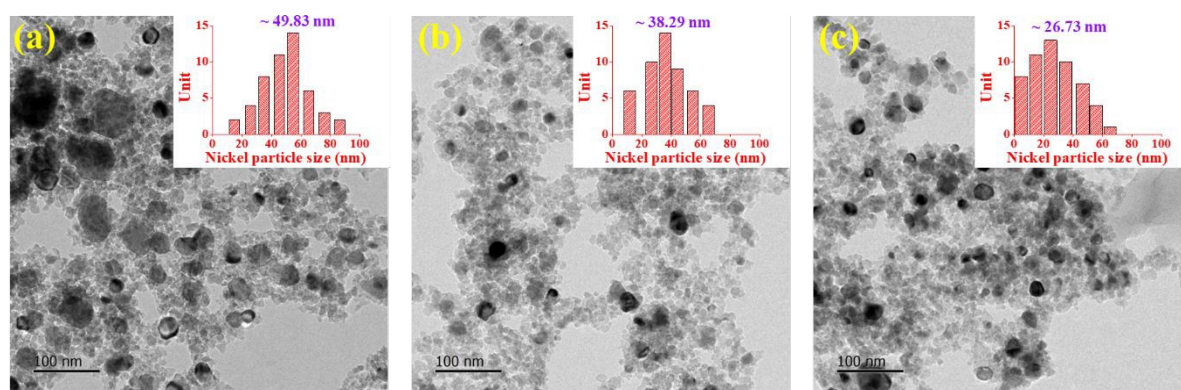


Fig. 4 – TEM images of the as-synthesized catalysts: (a) I-NMA, (b) O–NMA/Air, and (c) O–NMA/Inert/Air. The inset shows the NPs size distribution of the various catalysts.

The results of the ICP-OES analysis of the calcined samples are shown in Table S2. All the as-synthesized catalysts had nearly the same contents of Ni (18.2 ± 0.1 wt%), Mg (7.7 ± 0.1 wt%), and Al (34.2 ± 0.3 wt%), in agreement with the theoretical values. The excellent agreement between the experimental and theoretical values of the metal contents confirms that all of the Ni, Mg, and Al injected into the solution during the fabrication process was recovered in the solid catalyst after finishing the preparation process. Considering this paramount observation, the difference in the performances of the catalysts can be attributed to the difference in the catalysts' substructure and composition, such as BET SSA, nature of phases present, and extent of interaction between Ni active phase and support. This again highlights the essential role of inert annealing in modifying the catalyst substructure, where catalyst properties were greatly improved which would lead to much enhancement in the catalytic

performance towards the SMR reaction as will be discussed in the catalytic performance section. Especially, the high dispersion and small size of the Ni NPs are known to prevent the deposition of carbon species on the catalyst surface during the SMR reaction,⁴ leading to sustained high stability for long periods.

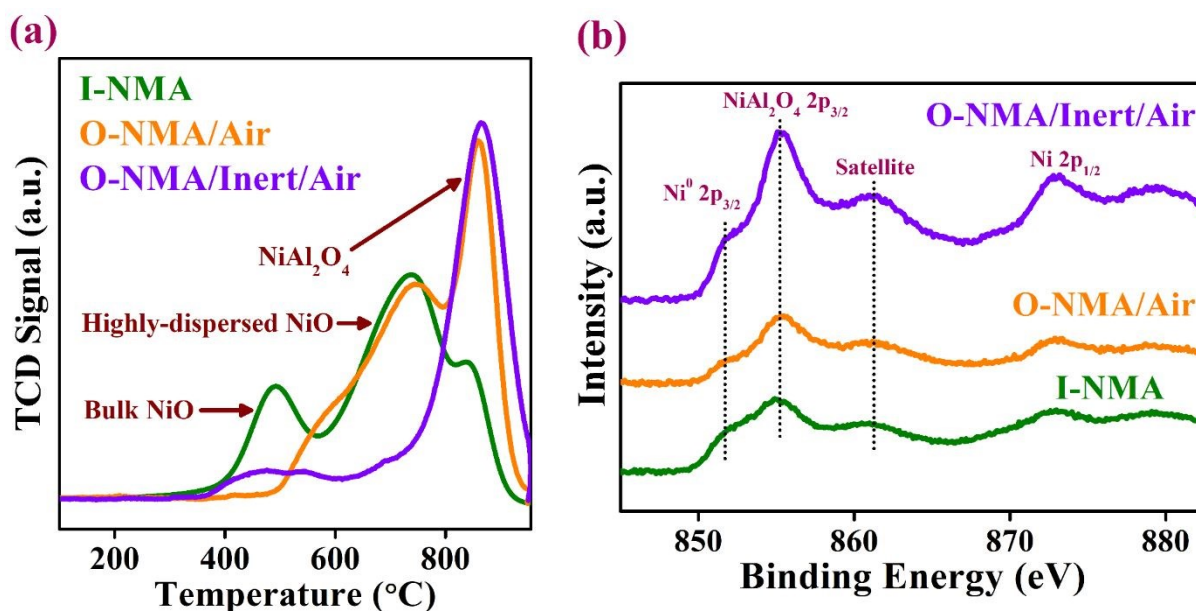


Fig. 5 – (a) H₂-TPR and (b) XPS spectra of mesoporous Ni/MgAl₂O₄ catalysts synthesized by different strategies.

Another important parameter for the high stability of catalysts is the strong metal-support interaction. This strong interaction plays a fundamental role in preventing Ni sintering during the SMR process, thus maintaining the catalytic activity for prolonged periods with high stability. H₂-TPR is an efficient technique for identifying the reducibility of metal-oxide-based supported catalysts and the degree of interaction between the active phase and support. H₂-TPR results suggest that the interaction of Ni NPs with the support is stronger in the O-NMA/Inert/Air catalyst than that in I-NMA and O-NMA/Air catalysts (Fig. 5a). I-NMA catalyst exhibited three reduction peaks at temperatures of 490, 735, and 836 °C, indicating the presence of different reducible Ni species with different interactions with the spinel support. The presence of a reduction peak at 490 °C in this sample is due to the reduction of bulk NiO

species, which weakly bounded with the support,³¹ in agreement with the XRD data (Fig. 3a).
The reduction peak at 735 °C, was related to the reduction of highly dispersed NiO species which strongly interact with the support.^{37,38} On the other hand, the presence of the reduction peak at higher temperature (836 °C) was ascribed to the reduction of the NiAl₂O₄ spinel,^{4,31,39,40} further confirming the existence of the NiAl₂O₄ phase in all catalysts, as had been demonstrated from the XRD analysis. When the one-pot strategy was applied for synthesizing the catalyst (O–NMA/Air), the reduction peak at 490 °C disappeared, and instead, a small shoulder appeared at a higher temperature (581 °C). The absence of reduction peaks in this catalyst at temperatures below 500 °C suggests the absence of the bulk NiO species, in agreement with the XRD data (Fig. 3a). The remaining two reduction peaks, which are attributed to the reduction of highly dispersed NiO and NiAl₂O₄, respectively shifted to higher temperatures of 752 and 859 °C, respectively. More importantly, the reduction peaks at 859 °C had the maximum intensity. All of these observations emphasize the great enhancement in the dispersion and interaction of Ni species with the support when the one-pot strategy is employed instead of the impregnation strategy, which indicates the importance of selecting the suitable route for synthesizing the SMR catalysts. In the case of the O–NMA/Inert/Air catalyst, there was only one very intense peak at 862 °C, which was ascribed to the reduction of NiAl₂O₄.⁴⁰ It is noteworthy to observe that the reduction peak in this catalyst had the maximum intensity and the maximum reduction temperature (862 °C). In contrast to the I–NMA and O–NMA/Air samples, which showed clear and intense peaks below the temperature of 800 °C, the O–NMA/Inert/Air catalyst showed only very weak peaks below 800 °C, which attributed to the reduction of the very small content of NiO existing in this catalyst as has been shown from the XRD (Figs. 3a) where there was a very small peak for NiO. Taking into account the aforementioned observations from the H₂-TPR profiles, it can be concluded that the majority of Ni species in the O–NMA/Inert/Air catalyst strongly linked to the mesoporous framework

of the spinel support. The H₂-TPR profiles of the O–NMA/Air and O–NMA/air_{4h} samples are presented in Fig. S2. Increasing only the calcination time from 2.0 to 4.0 h resulted in shifting the reduction peaks from 752 and 859 °C to 684 and 834 °C, respectively, indicating the weaker interaction between the Ni species and support in O–NMA/air_{4h} catalyst. This demonstrates the great importance of inert annealing in upgrading the structural properties of the catalyst.

The XPS analysis was performed to define the chemical states and electronic structures of the elements existing in the surface region of the catalysts (Fig. 5b). The XPS spectra of Ni 2p of the reduced catalysts show two main peaks at binding energies of 855.7 ± 0.1 and 873.2 ± 0.1 eV along with a shake-up satellite peak at around $861.5 \text{ eV} \pm 0.1$. In addition, there is a noticeable peak at 852.3 ± 0.1 eV, which is ascribed to the metallic Ni species.⁴² The binding energies of the Ni species in the catalysts are shown in Table S3. It is clear that the binding energies are almost same in all catalysts, indicating that the surface Ni was not influenced by altering the synthetic strategy, and its electronic environment was not changed. The existence of the Ni 2p_{3/2} peak and satellite peak at around 855.7 and 861.5 eV, respectively, for all samples is a typical characteristic of Ni species in the NiAl₂O₄ spinel.^{43,44} The binding energy of Ni 2p_{3/2} at around 855.7 eV is attributed to the Ni²⁺ species robustly interacted with the support,⁴⁵ suggesting that Ni⁰ and Ni²⁺ moieties coexisted on the surface of the reduced catalysts. This demonstrates that some proportion of Ni²⁺ was reduced to Ni⁰, while the rest proportion remained as Ni²⁺. Taking into account the existence of the oxidation state of the surface Ni in the form of Ni²⁺ and the fact that the binding energy of Ni 2p_{3/2} in pure NiAl₂O₄ is 856.0 eV,³¹ which is very close to 855.7 eV, it can be concluded that NiAl₂O₄ spinel species indeed exist within the surface of prepared catalysts, which agrees well with the XRD and H₂-TPR measurements. The binding energy of Ni 2p_{3/2} in pure NiO is about 854.4 eV^{31,44} which is much smaller than the value observed herein (855.7 eV) for the reduced catalysts. This indicates that the Ni 2p_{3/2} species exist in the form possessing strong interaction with the support which is

NiAl₂O₄ instead of NiO species. This further confirms the presence of NiAl₂O₄ spinel species in the herein synthesized materials. To clearly show the contents of reduced Ni species present within the surface region in the different catalysts, the deconvolution of the Ni XPS spectra was performed, and the data are shown in Fig. S3. It is obvious that the O–NMA/Inert/Air catalyst had the maximum peak intensity for Ni⁰ among the synthesized catalysts, indicating that it possessed the maximum quantity of metallic Ni on its surface, which is very beneficial for enhancing catalytic activity towards the SMR reaction. This further confirms the fundamental role played by the inert annealing step in upgrading the catalyst substructure where it led to increasing the content of reduced Ni species on the catalyst surface, which is very crucial for boosting the catalytic activity.

3.2 Catalytic performance

The SMR activities of the developed catalysts and the commercial catalyst at different GHSVs are plotted in Fig. 6 for the reaction conditions H₂O/CH₄= 3, *T*= 800 °C, and *P*= 1.0 atm. At the GHSV of 10,000 mL g_{cat}⁻¹ h⁻¹, all catalysts showed similar CH₄ conversion efficiencies until the stream time of 120.0 min. As the feed flow rate was increased from 10,000 to 40,000 mL g_{cat}⁻¹ h⁻¹, the CH₄ conversions of the as-prepared catalysts as well as the commercial catalysts decreased accordingly. As shown from Fig. 6, when the GHSV was increased from 10,000 to 40,000 mL g_{cat}⁻¹ h⁻¹, the drop in the CH₄ conversion efficiency was minimum for the O–NMA/Inert/Air catalyst: from 97.6 to 82.0%. The I–NMA and commercial catalysts showed conversion decreases from 97.5 and 98.0% to 68.8 and 67.0%, respectively. The deterioration in the catalytic conversion with increasing the gas feed-flow rate is attributed to the reduced reactant habitation time on the catalyst surface and the restricted access to active sites as a result of the increment in the number of reactants.⁴³ Moreover, coke formation on the surfaces of catalysts is enhanced by increasing the GHSV.⁴⁶ While the conversion efficiency remained almost constant as the GHSV was maintained constant, the O–NMA/Air catalyst

displayed a rapid degradation in its conversion efficiency at 40,000 mL $\text{g}_{\text{cat}}^{-1} \text{h}^{-1}$. It is clear that the O-NMA/Inert/Air catalyst maintained the highest conversion efficiency among the tested catalysts, indicating the best catalytic performance during the SMR reaction.

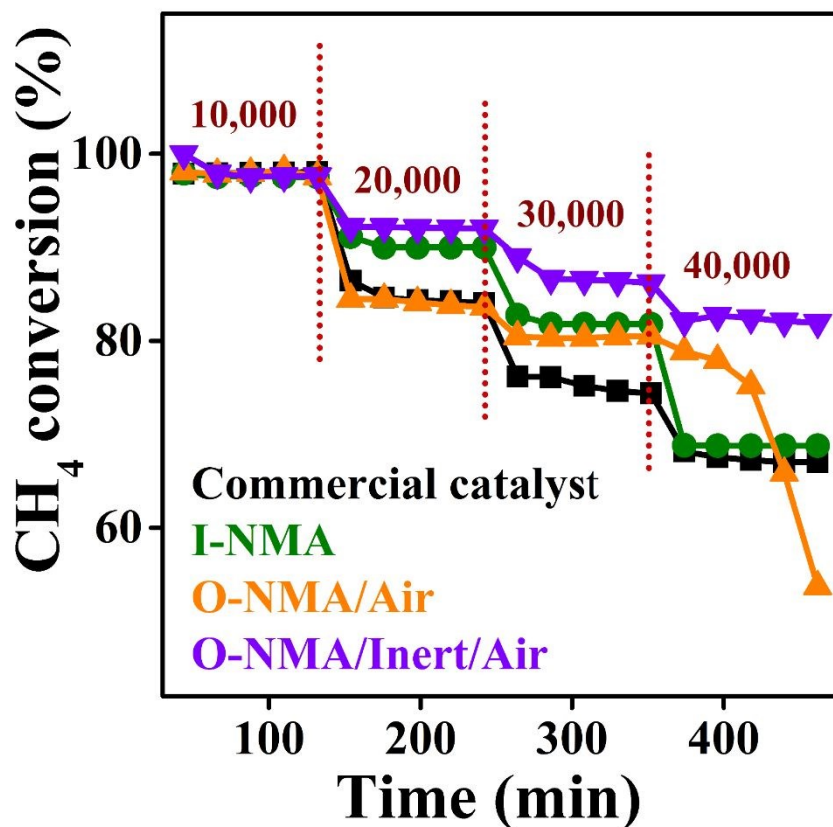


Fig. 6 – CH_4 conversions of mesoporous $\text{Ni/MgAl}_2\text{O}_4$ catalysts and commercial catalyst at different GHSVs ranging from 10,000 to 40,000 $\text{mL g}_{\text{cat}}^{-1} \text{h}^{-1}$.

Although the I-NMA and O-NMA/Inert/Air catalysts showed similar catalytic activity at the beginning of the reaction, they exhibited different activity with increasing the reaction time and GHSV: I-NMA showed a CH_4 conversion efficiency of 68.8% at the stream time of 480 min and GHSV of 40,000 $\text{mL g}_{\text{cat}}^{-1} \text{h}^{-1}$, whereas O-NMA/Inert/Air showed a CH_4 conversion efficiency of 82.0% at the same stream time. This result demonstrates the importance of selecting the proper synthetic strategy for designing an efficient catalyst for the SMR reaction. On the other hand, although the O-NMA/Air and O-NMA/Inert/Air catalysts were prepared by the same one-pot strategy except for the annealing step in the N_2 atmosphere

in the case of O–NMA/Inert/Air, they displayed different catalytic conversion efficiencies at the stream time of 480 min and GHSV of 40,000 mL g_{cat}⁻¹ h⁻¹ (53.7 and 82.0% for O–NMA/Air and O–NMA/Inert/Air, respectively), thus elucidating the significance of the inert annealing in boosting the reactivity of the catalyst during the SMR process. The O–NMA/Inert/Air catalyst displayed the highest H₂/CO ratios (Fig. S4) among the examined catalysts at various GHSVs ranging from 10,000 to 40,000 mL g_{cat}⁻¹ h⁻¹, which further confirms that this catalyst offered the best catalytic performance in the SMR reaction. In addition, Table S4 shows the comparison of SMR catalytic activity and stability of our catalyst (O–NMA/Inert/Air c) with that of similar composition reported in literature. It is obvious that O–NMA/Inert/Air catalyst is one of the top performing catalysts towards the SMR reaction. Base on the above physical characterization of the different catalysts, the superior catalytic performance of O–NMA/Inert/Air catalyst can be attributed to: (i) the large SSA with optimum mesoporosity and high pore volume, which drive to supplying more accessible Ni active sites for the gaseous reactants, (ii) the small size and high dispersion of Ni NPs throughout the catalyst infrastructure, (iii) the strong interaction between the Ni NPs and support, and hence suppressing the catalyst sintering and increasing the resistance to carbon deposition, and (iv) the high concentration of metallic Ni on the catalyst's surface as has been elucidated from the XPS analysis. The enrichment of catalyst surface with Ni⁰ could provide more catalytic active sites for the reaction between CH₄ and H₂O.

The most important objective of this study was to develop SMR catalyst with high resistance to coke formation under harsh operating conditions. We performed a catalytic reaction in the accelerated mode of coke formation under the conditions of H₂O/CH₄= 1, T= 700 °C, P= 1.0 atm., and GHSV= 10,000 mL g_{cat}⁻¹ h⁻¹ for 7.0 hours (Fig. S5). Under these SMR reaction conditions, I–NMA, O–NMA/Air, O–NMA/Inert/Air, and the commercial catalyst showed CH₄ conversions of 57.0, 59.3, 72.3, and 70.5%, respectively, which remained almost constant over the entire 7.0 h duration of the SMR reaction. The O–NMA/Inert/Air catalyst had

View Article Online
DOI: 10.1039/D1CY00485A

the highest CH₄ conversion efficiency among all the as-synthesized catalysts (Fig. S5a). Fig. S5b shows that the O–NMA/Inert/Air catalyst displayed the highest H₂/CO ratio, close to 3, which is the theoretical H₂/CO ratio. It also showed the highest value for carbon balance that would be ideally 1.0, meaning the least probability of coke deposition among the tested catalysts under the accelerated reaction conditions (Fig. S5c). The high durability of the O–NMA/Inert/Air catalyst is ascribed to the stable mesoporous substructure and the strong interaction between the active phase and support, as was confirmed from the BET, H₂-TPR, and H₂-chemisorption measurements. The excellent mesoporous structure facilitates the accessibility of the gaseous reactants to quickly reach the active sites existing within the catalyst substructure; meanwhile, the strong interaction of metallic Ni with the support inhibits the growth of NPs during the SMR reaction, thereby suppressing the coke formation, which easily occurs on larger NPs.

3.3. Characterization of used catalysts

The deposition of carbon in the form of filaments over the surfaces of all catalysts is shown in Fig. 7. As seen from Fig. 7a, the commercial catalyst displayed a very high density of coke, which almost fully covered its surface, revealing its weak resistance to carbon deposition and hence susceptibility to deactivation. On the other hand, the as-synthesized catalysts, especially O–NMA/Inert/Air, showed less affinity for carbon deposition, indicating their better resistance to coke formation. Raman spectroscopy was employed to identify the nature of carbon deposited on the surface of the catalysts after the SMR reaction (Fig. 8a). There were two distinct peaks in the Raman spectra at wavelengths of ~1344 and 1585 cm⁻¹, corresponding to the D and G bands.³² The first peak (D) is ascribed to the structural defects and lattice distortions in the sp³-hybridized carbon systems, and the second peak (G) is due to the in-plane vibrations of the sp²-bonded carbon atoms with a high degree of symmetry and graphitization. The intensity of the D band relative to the that of G band (I_D/I_G) has been used to characterize the degree of crystallinity and/or the existence of disorders in the carbon structure.³² The I–

NMA and O-NMA/Inert/Air catalysts showed high I_D/I_G ratios of 1.12 and 1.09, respectively, comparing to 0.71 for the O-NMA/Air catalyst. This demonstrated that the carbon deposited on the surface of the former catalysts was amorphous and contained high numbers of defects, meanwhile that deposited on the surface of the latter one had a high degree of crystallinity. The high graphitic degree of the deposited carbon could densely wrap the metallic Ni active sites, and hence leading to weakening the catalytic performance. It is noteworthy to observe that the carbon deposited on the surface of the O-NMA/Inert/Air catalyst had a very low degree of graphitization ($I_D/I_G = 1.09$) comparing to O-NMA/Air (0.71), which is advantageous in that the Ni-active sites were not fully blocked by the carbon deposited on its surface, meaning that the high catalytic activity could be sustained for longer periods over the O-NMA/Inert/Air catalyst than would be possible over the O-NMA/Air catalyst, indicating the significant role of the inert annealing in modifying the catalyst structure.

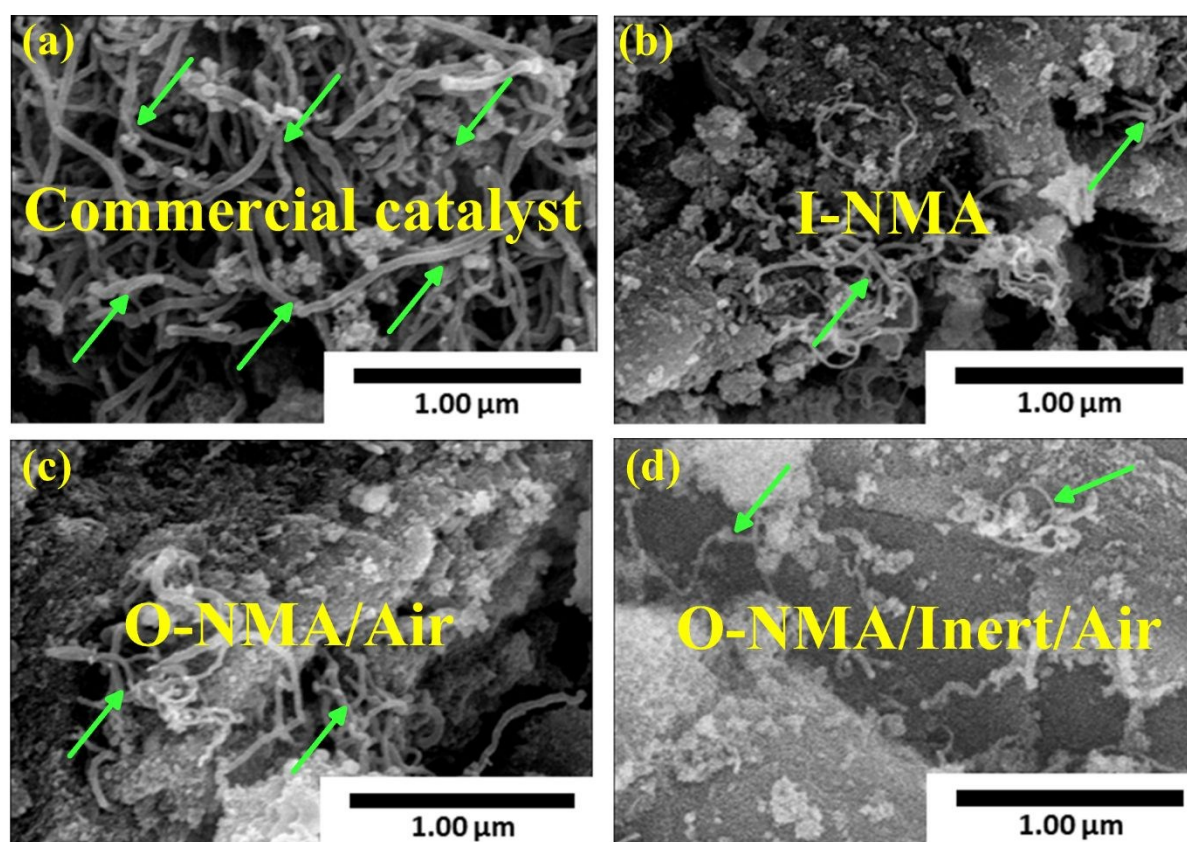


Fig. 7 – SEM images of the studied catalysts after the SMR reaction. The green arrows refer to the carbon filaments formed on the catalyst surface after the reaction.

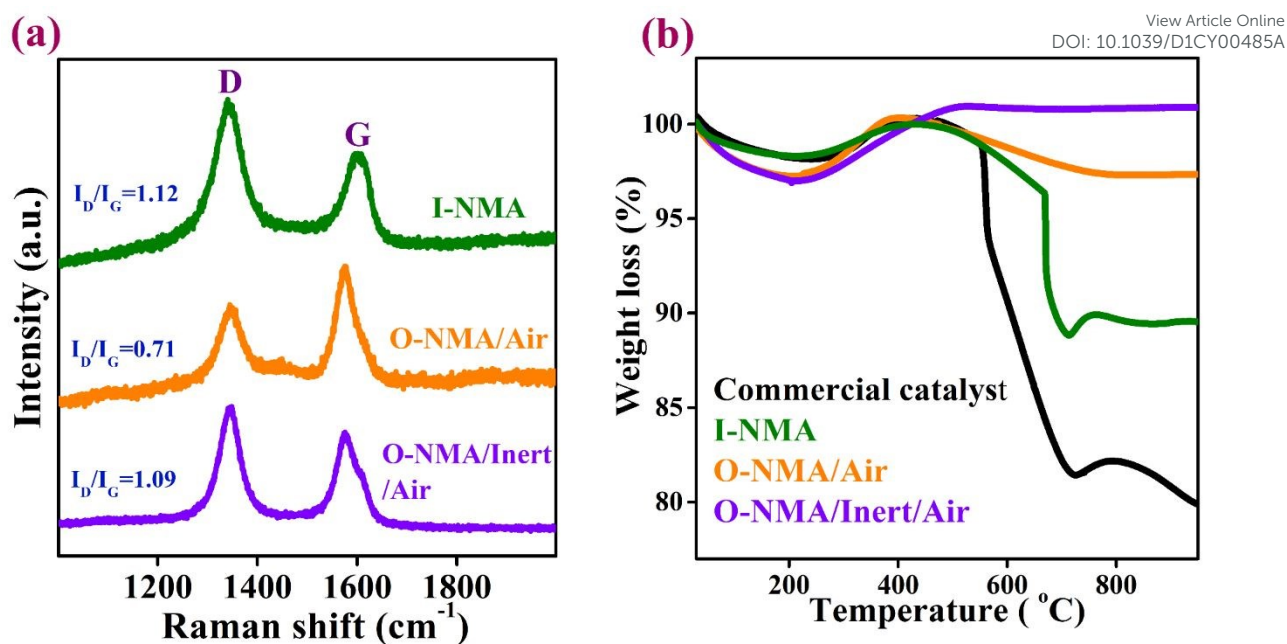
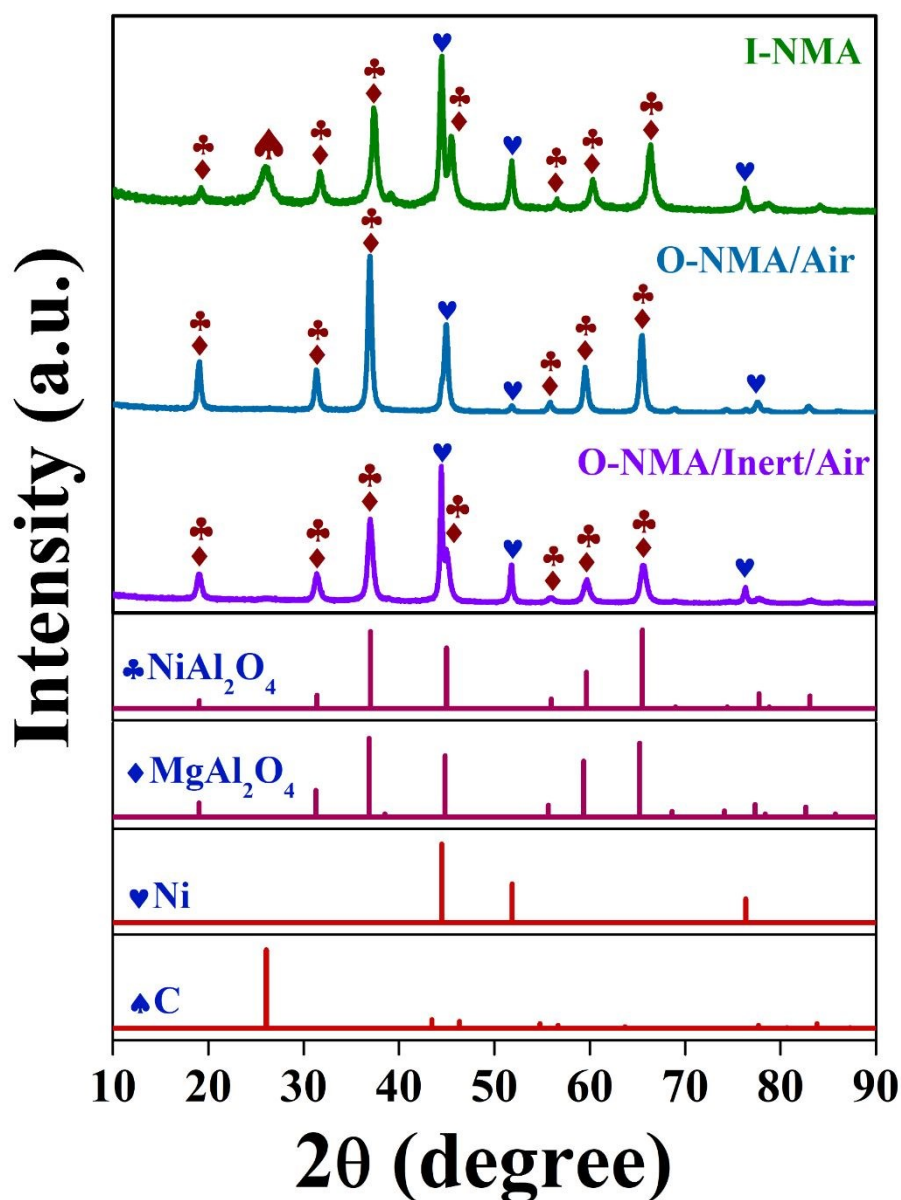


Fig. 8 – Raman spectra (a) and TGA (b) plots of mesoporous Ni/MgAl₂O₄ catalysts after the SMR reaction.

To determine the quantities of carbon species deposited on the surfaces of the used catalysts after performing the SMR reaction at 700 °C for 7.0 h ($H_2O/CH_4 = 1$ and $GHSV = 10,000 \text{ mL g}_{\text{cat}}^{-1} \text{ h}^{-1}$), a TGA analysis was done under air atmosphere, and the results are shown in Fig. 8b. The weight loss below 200 °C is attributed to the desorption of adsorbed moisture from the catalysts; meanwhile, the weight increase in the temperature range from 200 to about 400 °C is ascribed to the oxidation of metallic Ni species during the TGA experiments.⁴⁷ The weight-loss stage over 400 until 700 °C was due to the oxidation of carbon species deposited on the catalysts during the SMR reaction.⁴⁸ It is obvious that the weight loss was maximum in the commercial catalyst and minimum in O-NMA/Inert/Air, in well agreement with the FESEM data, where the amount of deposited carbon was very high in the former catalyst and very low in the latter one.



View Article Online
DOI: 10.1039/D1CY00485A

Fig. 9 – XRD plots of mesoporous Ni/MgAl₂O₄ catalysts fabricated by different strategies after the SMR reaction.

In order to get insights about the changes in the size of NPS after the SMR reaction, the XRD analysis of the used catalyst was done and the results are shown in Fig. 9. The calculated sizes of Ni NPs after the SMR reaction were found to be 52.34, 40.41, and 28.21 nm for I–NMA, O–NMA/Air, and O–NMA/Inert/Air, respectively comparing to 49.83, 38.29, and 26.73 nm, respectively for the same catalysts before the SMR reaction. It is obvious that there was a small increase in the size of the Ni NPs after performing the SMR reaction, indicating the strong

interaction between the Ni NPs and support, which is essential for minimizing the agglomeration of the NPs. It is also clear from the above figure that only I-NMA showed a clear carbon peak at 2θ of 26.1° , originated from the severe coke deposition, meanwhile the other catalysts did not show any obvious peaks for carbon.

4. Conclusions

Annealing the Ni/MgAl₂O₄ spinel catalyst in N₂ atmosphere before calcining it in air had a significant influence on its physicochemical properties. This step affords the following important advantages in terms of catalyst structure: 1) enhancing the SSA and mesoporosity leading to increased accessibility of reactants to active sites; 2) improving the dispersion of Ni NPs within the support and minimizing their size, and therefore, lowering the probability of coke formation, which easily occurs on large metallic NPs; 3) strengthening the interaction between the active phase (Ni) and the support, and thus preventing the catalyst sintering under the harsh working condition; 4) increasing the content of reduced Ni on the catalyst surface, and thereby providing more active sites for occurring the SMR reaction. As a result, the Ni/MgAl₂O₄ spinel catalyst subjected to an inert carbonization process before the calcination step in air displayed high CH₄ conversion efficiency, high durability, and excellent resistance for carbon deposition. The insights obtained from this study may have broad applications in developing Ni-based catalysts for various catalytic reactions such as water-gas shifting, reforming of hydrocarbons and oxygenates, CO₂ conversion, etc.

Acknowledgments

This research was funded by the framework of the research and development program of the Korea Institute of Energy Research (C0-2406). This research was also supported by Korea Electric Power Corporation (R20XO02-16).

References

1. J. X. Qian, T. W. Chen, L. R. Enakonda, D. B. Liu, J.-M. Basset and L. Zhou, *Int. J. Hydrogen Energy*, 2020, **45**, 15721–15743.
2. A. Al-Shahat Eissa, N. H. Kim and J. H. Lee, *J. Mater. Chem. A*, 2020, **8**, 23436–23454.
3. A. Iulianelli, S. Liguori, J. Wilcox and A. Basile, *Catal. Rev.*, 2016, **58**, 1–35.
4. S. Katheria, G. Deo and D. Kunzru, *Appl. Catal. A Gen.*, 2019, **570**, 308–318.
5. C.-j. Liu, J. Ye, J. Jiang and Y. Pan, *ChemCatChem*, 2011, **3**, 529–541.
6. E. Meloni, M. Martino and V. Palma, *Catalysts*, 2020, **10**, 352.
7. X. Yu, J. Zhang, X. Wang, Q. Ma, X. Gao, H. Xia, X. Lai, S. Fan and T.-S. Zhao, *Appl. Catal. B Environ.*, 2018, **232**, 420–428.
8. F. Wang, B. Han, L. Zhang, L. Xu, H. Yu and W. Shi, *Appl. Catal. B Environ.*, 2018, **235**, 26–35.
9. X. Zhai, S. Ding, Z. Liu, Y. Jin and Y. Cheng, *Int. J. Hydrogen Energy*, 2011, **36**, 482–489.
10. M. Zhang, J. Zhang, Z. Zhou, S. Chen, T. Zhang, F. Song, Q. Zhang, N. Tsubaki, Y. Tan and Y. Han, *Appl. Catal. B Environ.*, 2020, **264**, 118522.
11. K. Bu, J. Deng, X. Zhang, S. Kuboon, T. Yan, H. Li, L. Shi and D. Zhang, *Appl. Catal. B Environ.*, 2020, **267**, 118692.
12. Q. Wei, X. Gao, L. Wang and Q. Ma, *Fuel*, 2020, **271**, 117631.
13. Y. Xu, T. Hirano, H. Kunieda, Y. Hara and Y. Miyata, *Catal. Sci. Tech.*, 2020, **10**, 2004–2019.
14. M. Li and A. C. van Veen, *Appl. Catal. A Gen.*, 2018, **550**, 176–183.
15. M. Usman, W. M. A. Wan Daud and H. F. Abbas, *Renew. Sustain. Energy Rev.*, 2015, **45**, 710–744.

16. R. Dębek, M. Motak, M. E. Galvez, T. Grzybek and P. Da Costa, *Appl. Catal. B Environ.*, 2018, **223**, 36–46. View Article Online
DOI: 10.1039/D1CY00485A
17. N. Wang, Z. Xu, J. Deng, K. Shen, X. Yu, W. Qian, W. Chu and F. Wei, *ChemCatChem*, 2014, **6**, 1470–1480.
18. X. Fang, C. Peng, H. Peng, W. Liu, X. Xu, X. Wang, C. Li and W. Zhou, *ChemCatChem*, 2015, **7**, 3753–3762.
19. L. Xu, H. Song and L. Chou, *Catal. Sci. Tech.*, 2011, **1**, 1032–1042.
20. A. Chatla, M. M. Ghouri, O. W. El Hassan, N. Mohamed, A. V. Prakash and N. O. Elbashir, *Appl. Catal. A Gen.*, 2020, **602**, 117699.
21. S. A. Theofanidis, V. V. Galvita, H. Poelman, N. V. R. A. Dharanipragada, A. Longo, M. Meledina, G. Van Tendeloo, C. Detavernier and G. B. Marin, *ACS Catal.*, 2018, **8**, 5983–5995.
22. S.-A. Theofanidis, J. A. Z. Pieterse, H. Poelman, A. Longo, M. K. Sabbe, M. Virginie, C. Detavernier, G. B. Marin and V. V. Galvita, *Appl. Catal. B Environ.*, 2020, **267**, 118691.
23. S. A. Theofanidis, V. V. Galvita, H. Poelman and G. B. Marin, *ACS Catal.*, 2015, **5**, 3028–3039.
24. S. A. Theofanidis, V. V. Galvita, H. Poelman, R. Batchu, L. C. Buelens, C. Detavernier and G. B. Marin, *Appl. Catal. B Environ.*, 2018, **239**, 502–512.
25. S. Damyanova, B. Pawelec, K. Arishtirova and J. L. G. Fierro, *Int. J. Hydrogen Energy*, 2012, **37**, 15966–15975.
26. L. C. Buelens, A. N. V. R. Dharanipragada, H. Poelman, Z. Zhou, G. B. Marin and V. V. Galvita, *J. CO₂ Util.*, 2019, **29**, 36–45.
27. V. K. Jaiswar, S. Katheria, G. Deo and D. Kunzru, *Int. J. Hydrogen Energy*, 2017, **42**, 18968–18976.

28. J.-C. Zhang, B.-H. Ge, T.-F. Liu, Y.-Z. Yang, B. Li and W.-Z. Li, *ACS Catal.*, 2020, **10**, 783–791. Article Online
DOI: 10.1039/D1CY00485A
29. J. Guo, H. Lou, H. Zhao, D. Chai and X. Zheng, *Appl. Catal. A Gen.*, 2004, **273**, 75–82.
30. E. N. Alvar and M. Rezaei, *Scr. Mater.*, 2009, **61**, 212–215.
31. Q. Wei, X. Gao, G. Liu, R. Yang, H. Zhang, G. Yang, Y. Yoneyama and N. Tsubaki, *Fuel*, 2018, **211**, 1–10.
32. A. A. Eissa, S. G. Peera, N. H. Kim and J. H. Lee, *J. Mater. Chem. A*, 2019, **7**, 16920–16936.
33. G. Mistura, A. Pozzato, G. Greci, L. Bruschi and M. Tormen, *Nat. Commun.*, 2013, **4**, 2966.
34. D. Xia, Y. Chen, C. Li, C. Liu and G. Zhou, *Int. J. Hydrogen Energy*, 2018, **43**, 20488–20499.
35. K. Jabbour, A. Saad, L. Inaty, A. Davidson, P. Massiani and N. El Hassan, *Int. J. Hydrogen Energy*, 2019, **44**, 14889–14907.
36. K. Jabbour, P. Massiani, A. Davidson, S. Casale and N. El Hassan, *Appl. Catal. B Environ.*, 2017, **201**, 527–542.
37. R. L. B. A. Medeiros, G. P. Figueredo, H. P. Macedo, Â. A.S. Oliveira, R. C. Rabelo-Neto, D. M. A. Melo, R. M. Braga and M. A. F. Melo, *Fuel*, 2021, **287**, 119511.
38. Z. Taherian, V. Shahed Gharahshiran, A. Khataee, F. Meshkani and Y. Orooji, *Catal. Commun.*, 2020, **145**, 106100.
39. L. Smoláková, M. Kout, E. Koudelková and L. Čapek, *Ind. Eng. Chem. Res.*, 2015, **54**, 12730–12740.
40. B. Jin, S. Li and X. Liang, *Fuel*, 2021, **284**, 119082.
41. Y.-L. Lee, B.-J. Kim, H.-R. Park, S.-Y. Ahn, K.-J. Kim and H.-S. Roh, *J. CO₂ Util.*, 2020, **42**, 101354.

42. K. Han, W. Yu, L. Xu, Z. Deng, H. Yu and F. Wang, *Fuel*, 2021, **291**, 120182. View Article Online
DOI: 10.1039/D1CY00485A
43. L. Xu, H. Song and L. Chou, *ACS Catal.*, 2012, **2**, 1331–1342.
44. L. Li, M. Huo, Y. Zhang and J. Li, *J. Porous Mater.*, 2017, **24**, 1613–1625.
45. B. Li, Y. Luo, B. Li, X. Yuan and X. Wang, *Fuel Process. Technol.*, 2019, **193**, 348–360.
46. Y. Khani, Z. Shariatinia and F. Bahadoran, *Chem. Eng. J.*, 2016, **299**, 353–366.
47. F. Wang, K. Han, W. Yu, L. Zhao, Y. Wang, X. Wang, H. Yu and W. Shi, *ACS Appl. Mater. Interfaces*, 2020, **12**, 35022–35034.
48. B. Han, L. Zhao, F. Wang, L. Xu, H. Yu, Y. Cui, J. Zhang and W. Shi, *Ind. Eng. Chem. Res.*, 2020, **59**, 13370–13379.